General Disclaimer

One or more of the Following Statements may affect this Document

- This document has been reproduced from the best copy furnished by the organizational source. It is being released in the interest of making available as much information as possible.

- This document may contain data, which exceeds the sheet parameters. It was furnished in this condition by the organizational source and is the best copy available.

- This document may contain tone-on-tone or color graphs, charts and/or pictures, which have been reproduced in black and white.

- This document is paginated as submitted by the original source.

- Portions of this document are not fully legible due to the historical nature of some of the material. However, it is the best reproduction available from the original submission.

DRA/ MARSHALL

SIMULATION OF SOLIDIFICATION IN A BRIDGMAN CELL

Interim Report Contract No. NAS8-35331

For

National Aeronautics and Space Administration

George C. Marshall Space Flight Center

Marshall Space Flight Center, AL 35812

From

Continuum, Inc.

Youssef M. Dakhoul

Richard C. Farmer

4715 University Drive, Suite 118

August 22, 1984

ACKNOWLEDGEMENTS

The study described herein was performed for the Semiconductors and Devices Branch of the Space Processing Division at the National Aeronautics and Space Administration's Marshall Space Flight Center. The interest of the Technical Monitors, S.L. Lehoczky, F.R. Szofran and E.K. Cothran, is greatly appreciated

INTRODUCTION

Bridgman-type crystal growth techniques are attractive methods for producing homogeneous, high-quality infrared detector and junction device materials. However, crystal imperfections and interface shapes still must be controlled through modification of the temperature and concentration gradients created during solidification. The objective of this investigation was to study the temperature fields generated by various cell and heat-pipe configurations and operating conditions. Continuum's numerical model of the temperature, species concentrations, and velocity fields (1) was used to describe the thermal characteristics of Bridgman cell operation. Detailed analyses of the other transport processes will be addressed in subsequent phases of this research program.

Alloy in the Bridgman cell is melted by an enclosing furnace (a high temperature heat-pipe); the alloy is solidified by slowly replacing the heated walls with cooler walls. Radiative exchange between the furnace walls and the alloy is a primary means of heat transfer, as is the conduction of heat along the glass ampule wall. Tailoring of cell operation by control of the heat transfer process is described qualitatively in (2). This study will address cell design by quantitative evaluation of the thermal features of the system.

Experimental studies by Lehoczky and Szofran of Cd/Hg/Te alloys in Bridgman cells (3) and of the phase equilibrium behavior of these alloys (4) indicate that an HgTe enriched layer should accumulate on the melt side of the interface, hence both thermal and solutal density gradients would tend to stablize the fluid and prevent buoyant convection. Furthermore, local measurements of crystal composition showed significant radial variation (3). Measured axial composition variations were interpreted in terms of phase equilibrium relationships and axial diffusion, but the radial variations were attributed to other factors. The implication is that radial temperature gradients must affect the shape of the melt/solid interface and, thus, create thermal and/or solutal currents. This study predicted melt/solid interface and isotherm shapes for a variety of wall heating conditions. Velocity and species distribution effects were not considered in this work, although momentum and species conservation equations are already included in the Bridgman cell model. The very complex heat transfer boundary conditions for the cell must be accurately modeled before it is meaningful to attempt predictions of the convective flow caused by curved interface shapes.

The geometry shown in Figure 1 is complex and does not lend itself to parametric analyses. Rather cell and furnace dimensions reported in reference (3) will be used exclusively and parametrics were reserved for surface radiative properties and glass transmissivity, which are the least well known of the important thermal properties of the system. Effects controlled by system operating conditions such as the hot and cold heat pipe temperatures and growth rates were investigated.

The analyses performed and the predicted results are presented in the remainder of this report. Critical design conditions were identified for further study in the later phases of this research program.

TECHNICAL DISCUSSION

A thermal analysis of the Bridgman cell was made for the axisymmetric, quasi-steady system shown in Figure 1. The energy equation was solved for both the molten and solid alloy regions. Solidification was assumed to occur at a fixed temperature. One-dimensional species solutions were used to estimate the effect of composition on melt thermal conductivity, otherwise the energy equation solution from Continuum's Bridgman cell model was used. Boundary conditions along the glass wall are complex due to (a) the necessity of treating the glass with a lumped parameter model (or as a separate computational region) to determine the temperature distribution within the glass with sufficient accuracy to evaluate the heat conduction to the alloy and (b) the integral nature of the radiation flux in the annular space between the furnace and the alloy requiring a major assumption (or a three-dimensional view factor evaluation and an axial integration of the heat flux). The simplified flux equation was used in this study to expedite generating a wider range of parametric results for an initial thermal analysis. Details of the calculations and a description of the alloy properties used are given in subsequent paragraphs; followed by a presentation of parametric cases which were studied. Two types of analyses were made: in the first, simple heat conduction within the cell was predicted for specified wall temperatures to compare to solutions which have been reported by Naumann and Lehoczky (5) and, in the second, various wall heating conditions were studied.

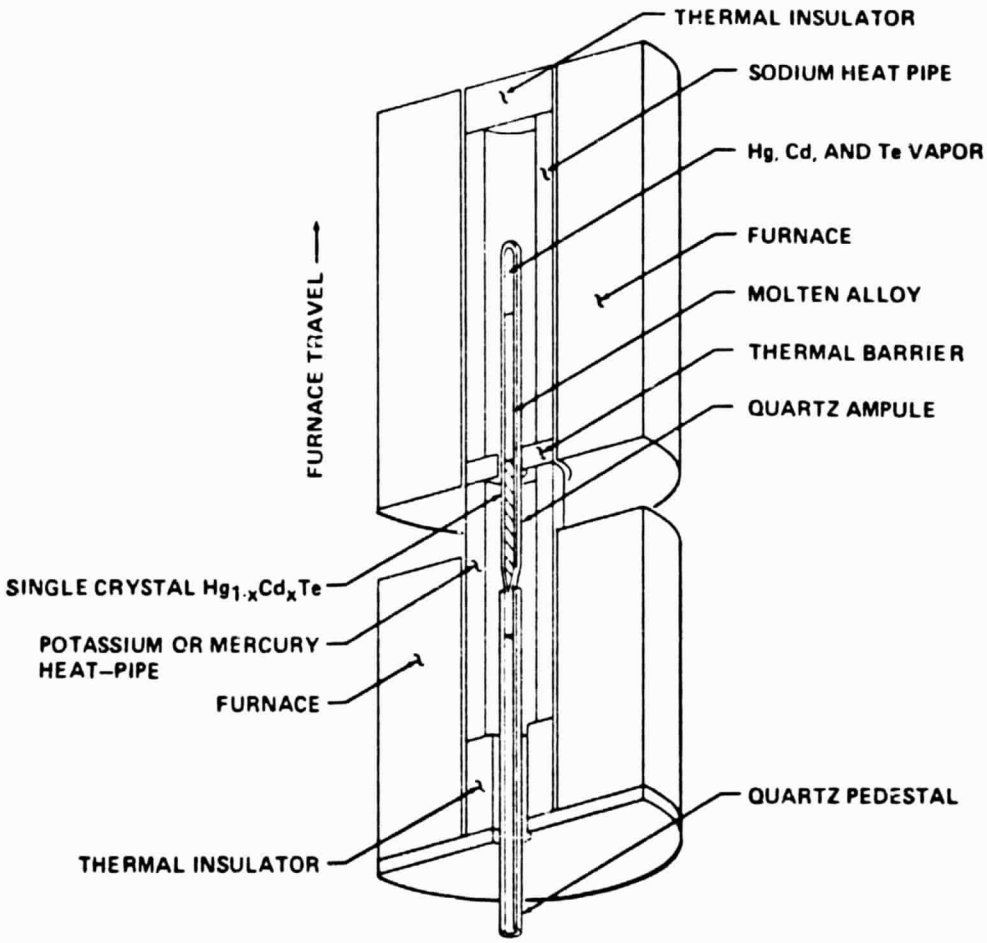

Figure 1: Bridgman Crystal Growth Furnace Assembly
From Ref. (3)

Continuum's VAST code was used as the basic Bridgman cell model (1). Options of including radiation and conduction to the cell walls, as well as conduction and transmission through the fused silica walls of the ampule are available. The top and bottom ends of the ampule are too far removed from the interface to effect the temperature field in the vicinity of the interface, therefore temperature boundary conditions are appropriate at these locations. The VAST code is a numerical solution to the species, momentum, and energy equations. The analog utilizes an explicit time integration to produce a steady-state solution for a nodal network which is obtained from a finite-element formulation. For this study, only the energy equation solution was used. The Bridgman cell model contains a detailed specification of boundary conditions to describe heating through the glass wall and from the furnace walls; these boundary conditions directly couple the environmental conditions of the alloy in the cell to the node temperatures along the outermost edge of the alloy. The only time effect considered was to specify the molten alloy thermal conductivity as a function of growth rate, therefore the only significant thermal effect omitted from this model is the heat of fusion which is a direct function of growth rate. A more accurate analysis cannot be obtained without also solving the species equations.

PHYSICAL PROPERTIES OF THE Hg/Cd/Te SYSTEM

Best available physical property data for the Hg/Cd/Te system are summarized in (1); however, to expedite an initial thermal analysis study, some simplification and empirical curve fits of these data were used. The following alloy properties were used for this study. The density of $Hg_{1-x}\ Cd_x\ Te$ alloy was assumed constant in all calculations and equal to 7.54 gm/cm^3. This corresponds to a liquid phase mole fraction, x, of 0.2 which is the initial composition. Density variations are neglected since convective motions inside the ampule are not considered.

The local alloy composition, x, is calculated at each node in the liquid phase using the following one-dimensional species solution (6):

$$x = x_0 \left\{ 1 - \frac{S-1}{S} \exp(-RZ/D) \right\} \qquad (\text{for } Z \geq 0)$$

where S is a segregation coefficient equal to 3.9; R is the growth rate; D is an effective diffusion coefficient equal to 5.5 E-5 cm^2/sec; and Z is the vertical distance above the melting isotherm which is easily determined from the temperature distribution. According to the above equation, x is equal to x_0/S at $Z = 0$ and changes exponentially in Z to approach x_0 as Z becomes large. In the solid phase ($Z < 0$), the composition is assumed constant and equal to x_0.

The thermal conductivity, K, is calculated at each node in the liquid phase using the following equations (5):

$$\alpha = B\,(\ln(T)) - A$$

$$K = \alpha\,\rho\,C_p$$

where α is the thermal diffusivity; T is temperature in °C; ρ is the constant density (7.54 gm/cm^3); C_p is the heat capacity (1.8428 E 6 $cm^2/sec^2\,°K$). The empirical coefficients A and B are given in Table 1 as functions of composition, x. In the solid phase, the thermal conductivity is assumed constant and equal to 6.3947 E 4 gm cm/sec^3 °K. The heat of fusion was neglected in this analysis.

Table 1. Values of the Empirical Coefficients A and B. Data from Ref. (6)

x	A	B
0.	67.401	10.4655
0.052	46.767	7.25493
0.107	46.024	7.09724
0.205	42.041	6.44051
0.301	37.423	5.69691

BOUNDARY CONDITIONS FOR A BRIDGMAN CELL

Thermal energy is exchanged between the alloy and the furnace, through the glass wall of the ampule, by radiation and conduction. A part of the radiated energy is directly transmitted to the alloy while the glass wall absorbs the remaining part and reflects a negligible amount. The radiant energy absorbed by the glass, along with the energy conducted through the air gap, is conducted through the two-dimensional domain of the glass wall. A part of this conducted energy reaches the alloy, while the remaining part flows in the longitudinal direction. The net result is a certain amount of energy reaching or leaving the outer surface of the alloy per unit area per unit time. An accurate evaluation of this energy flux is vital for predicting a correct temperature distribution within the alloy. Once calculated, this energy flux, Q, can easily be used to impose the proper boundary condition on the solution of the energy equation.

In order to calculate the boundary heat flux, Q, a "lumped" heat balance is performed on the portion of the glass wall associated with each boundary node (see Figure 2). This element of glass is assumed to have a uniform temperature T_a which is an average of the node temperature, T_n, and the temperature of the outer surface of the ampule at a point facing the node, T_g. T_n is obtained from the solution of the energy equation at the previous time iteration and T_g is calculated by equating the heat conducted to and through the air/glass interface:

$$(K_a/\delta_a)\ (T_f - T_g) = (K_g/\delta_g)\ (T_g - T_n)$$

where K_a and K_g are the conductivities of air and glass; δ_a and δ_g are widths of the air gap and glass wall; and T_f is the furnace temperature at a point facing the node. In a similar manner, T_{aa} and T_{ab} are calculated to represent average temperatures in the glass portions above and below the portion under consideration.

The set of temperatures T_f, T_g, T_a, T_n, T_{aa} and T_{ab} is used to calculate the following heat fluxes:

$$Q_a = (K_g/\delta_{za})\ (T_{aa} - T_a)$$

$$Q_b = (K_g/\delta_{zb})\ (T_{ab} - T_a)$$

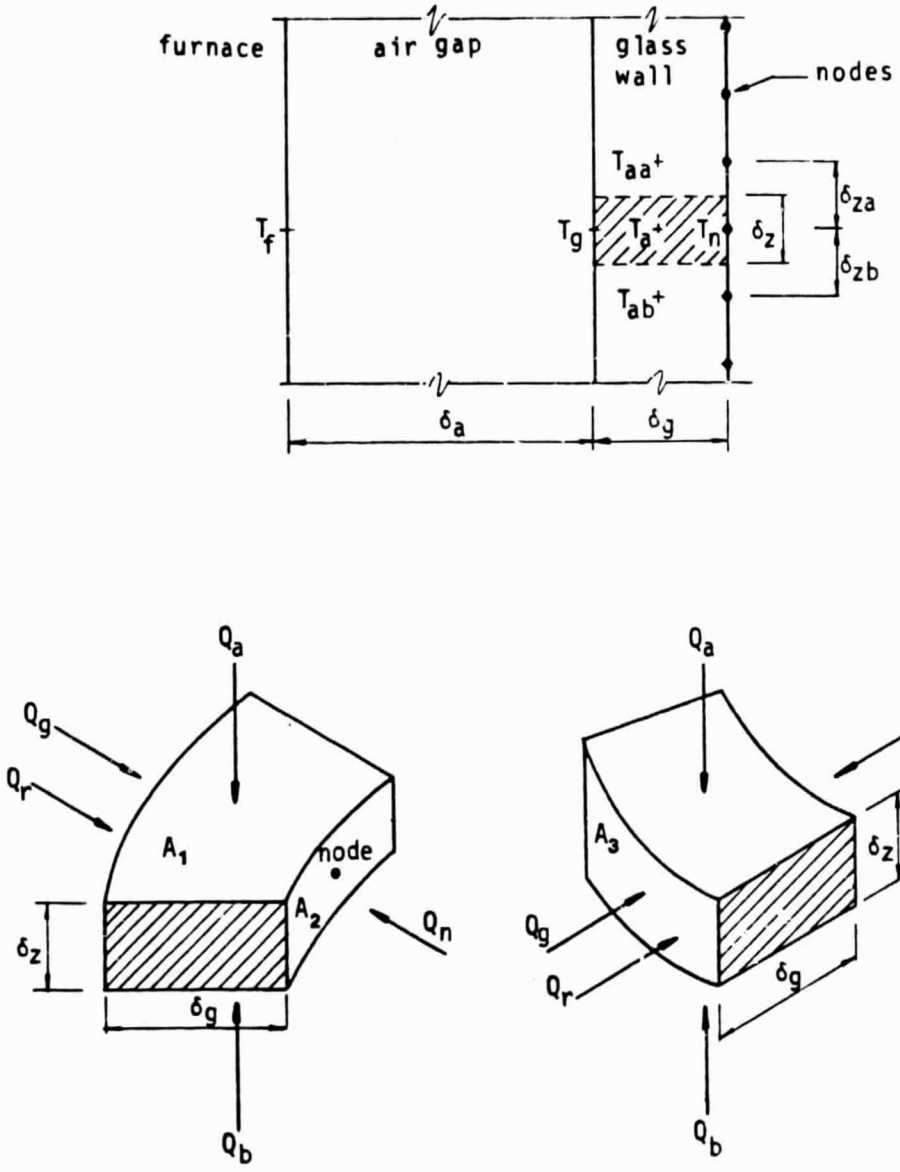

Figure 2: Schematic Presentation of the Boundary Conditions.

$$Q_g = (2 K_g/\delta_g) (T_g - T_a)$$

$$Q_n = (2K_g/\delta_g) (T_n - T_a)$$

$$Q_r = H_r (T_f^4 - T_a^4)$$

$$Q_r(\text{absorbed}) = Q_r(1 - \tau)$$

$$Q_r(\text{transmitted}) = Q_r\tau$$

where τ is the transmissivity of the glass, and H_r is a radiation coefficient the value of which is discussed later. In each of the above formulae, K_g is the glass conductivity at a temperature equal to the average of the pair of temperatures used to calculate the flux. Also, τ is the transmissivity of the glass at a temperature equal to $(T_f + T_a)/2$. Figure 3 shows the temperature dependency of K_a, K_g and τ.

The energy fluxes cause the temperature of the glass element to change from T_a to T_a'. The new T_a' is calculated from the heat balance on the glass "lump":

$$(V_g\rho_g C_g/\Delta t) (T_a' - T_a) = (Q_a + Q_b) A_1 + (Q_g + Q_r(\text{absorbed}))A_3 + Q_n A_2$$

where V_g is the volume of the glass element; ρ_g is the density of the glass ($2.203 gm/cm^3$); C_g is the specific heat of glass; and Δt is the time step size. The areas A_1, A_2 and A_3 are shown in Figure 2. Finally, the flux Q which represents the energy exchange between the furnace and the outer surface of the alloy in the vicinity of the node is calculated as:

$$Q = (2K_g/\delta_g) (T_a' - T_n) + Q_r(\text{transmitted})$$

At each boundary node, the energy per unit volume ρE_{old} (obtained by solving the energy equation) is adjusted to accommodate the flux Q as follows:

$$\rho E_{new} = \rho E_{old} + Q A_2 \Delta t/v$$

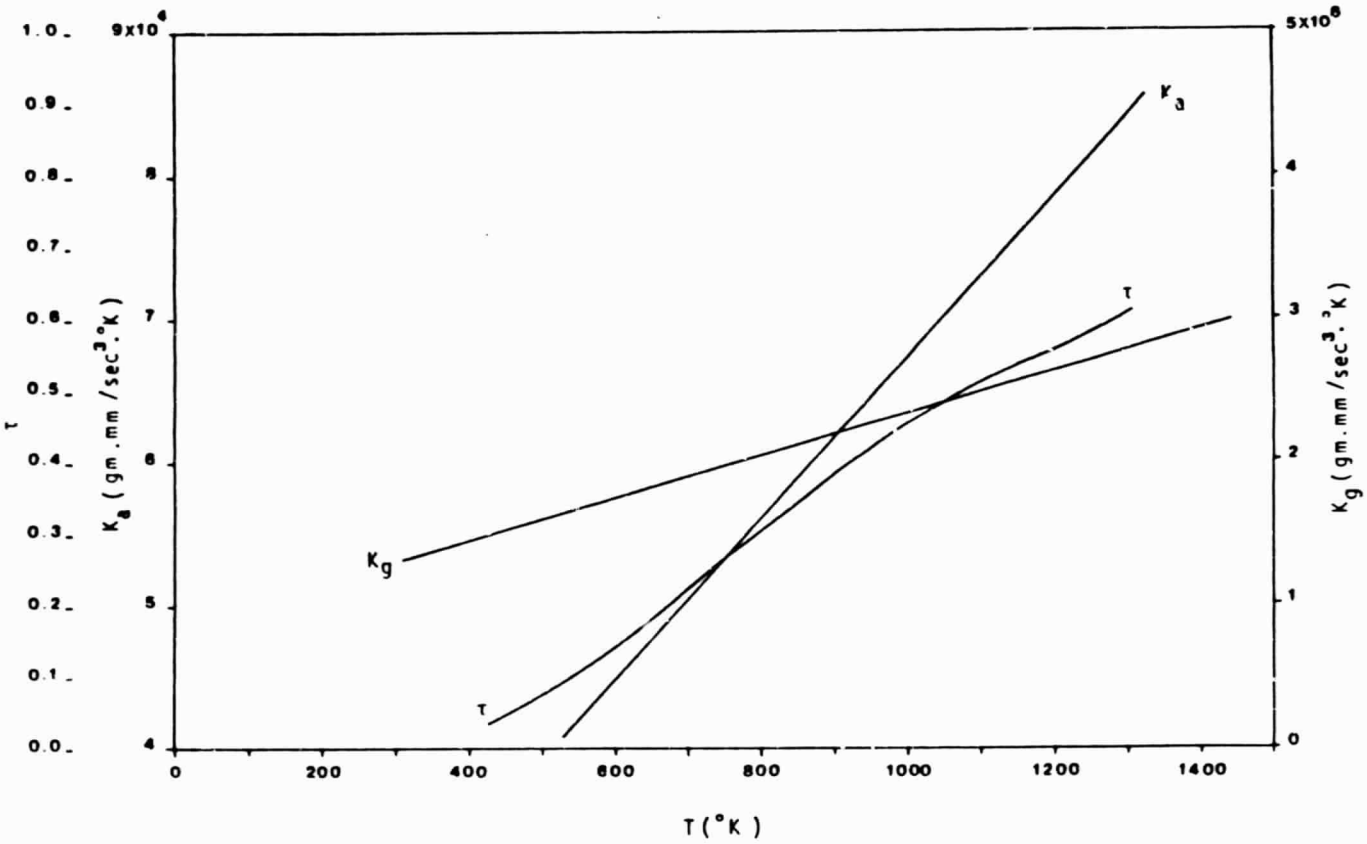

Figure 3: Properties of air and glass at different temperatures.
Data from Reference (6).

Where v is the volume of the alloy element associated with the node. This energy adjustment is performed at the end of each time step.

In calculating the radiative heat flux, Q_r, a radiation coefficient, H_r is used. To estimate H_r, the following assumptions are made:

1. The area A_2 (see Figure 2) is a gray surface with a uniform temperature of T_a.

2. The area A_2 "sees" a furnace area, A_f, which is also a gray surface at a uniform temperature of T_f. This is a reasonable approximation since A_2 sees primarily that part of the furnace radially facing it. T_f is taken to be the hot furnace temperature for all nodes above the barrier, and the cold furnace temperature for all nodes below the barrier. For the nodes facing the barrier, T_f varies linearly between the hot and cold temperatures.

3. Both A_2 and A_f satisfy Kirchhoff's Law, i.e. the absorptivity, a, is equal to the emissivity, ϵ.

Based on these assumptions, the idealized gray-body heat balance (7) is used:

$$Q_r = \sigma \left(T_f^4 - T_a^4\right) / \left\{(A_2/A_f)\ (\rho_f/\epsilon_f) + 1/F + (\rho_{al}/\epsilon_{al})\right\}$$

where σ is the Stefan-Boltzmann constant (5.6696×10^{-5} gm/sec^3 °K^4); ρ_f and ρ_{al} are reflectivities; ϵ_f and ϵ_{al} are emissivities of the furnace and the alloy's surface respectively. F is a view factor between A_2 and A_f. Since A_2 "sees" A_f and nothing else, F is equal to 1. Furthermore, the furnace area A_f, which is much larger than the elemental area A_2, has a large emissivity and a small reflectivity. Thus, the term $(A_2/A_f)\ (\rho_f/\epsilon_f)$ is neglected and an approximation of H_r is given by:

$$H_r = \sigma / \left\{1 + (\rho_{al}/\epsilon_{al})\right\}$$

Using $\epsilon_{al} = 0.2$ and $\rho_{al} = 0.8$, the estimated value of H_r becomes 1.1×10^{-5} (gm/sec^3 °K^4). The value of H_r obviously controls the efficiency of the radiative exchange between the furnace and the alloy. Using H_r as a parameter should demonstrate the impact of the radiation mode of heat transfer on the calculated temperature field within the alloy.

The radiative energy exchange between the furnace and the alloy can be modeled more precisely by an expression for the net energy radiated from a differential area on the furnace to a differential area on the alloy's surface per unit time. Intergrating this expression over A_2 and over the furnace area "seen" by it gives an accurate value of the radiant energy reaching A_2 per unit of time. The determination of whether or not this method appreciably improves the accuracy of the radiation model is the subject of a subsequent investigation by Continuum.

PARAMETRIC STUDIES

The model described above was solved, using Continuum's work station facilities, for a wide range of input parameters. The calculations are divided into four groups of runs. The first group is intended to verify the performance of the model by requiring it to duplicate an appropriate analytical solution. Each of the last three groups is designed to investigate the effect of a certain input parameter on the alloy's temperature distribution at the steady state.

The first group consists of two runs. In Run #1, the case of infinite solid cylinder, with constant conductivity and a given surface temperature, is simulated. Therefore, neither the composition calculations nor the boundary conditions described above are invoked, but the energy equation is numericaly solved in the axisymmetric domain with a specified set of temperatures at the surface nodes. Run #2 differs from Run #1 in that the conductivity of the material drops from 7K to K at all locations where the temperature is less that 700 °C . The specific value of K has no effect on the results. Figure 4 shows a comparison between the analytical solution reported in reference (5) and Continuum's solution.

Run #1

Constant thermal conductivities in liquid and solid phases.

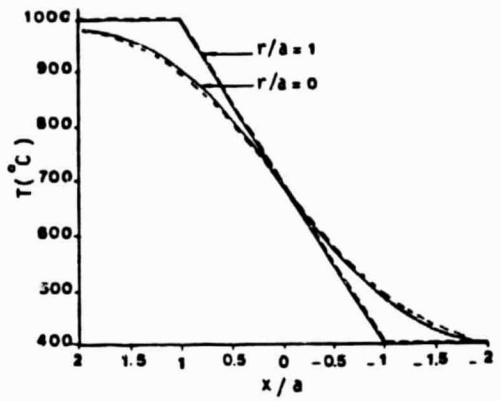

Axial thermal profiles

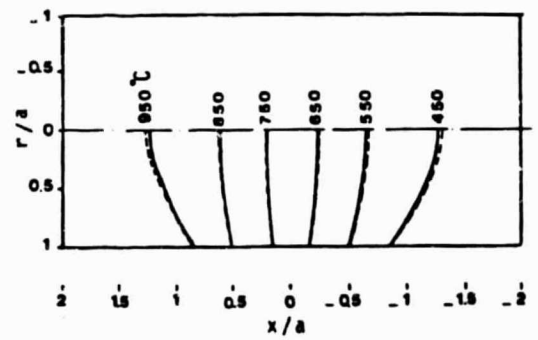

Two-Dimensional temperature distribution

Run #2

Liquid phase conductivity is 7 times larger than solid phase conductivity.

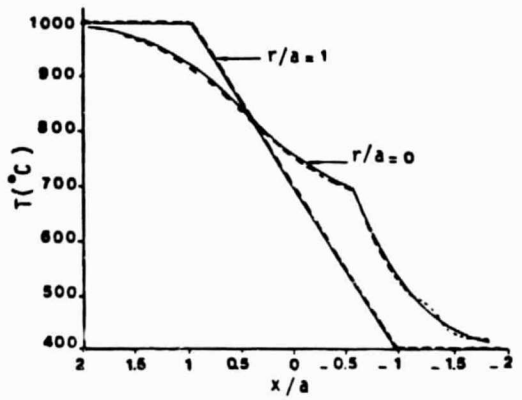

Axial thermal profiles

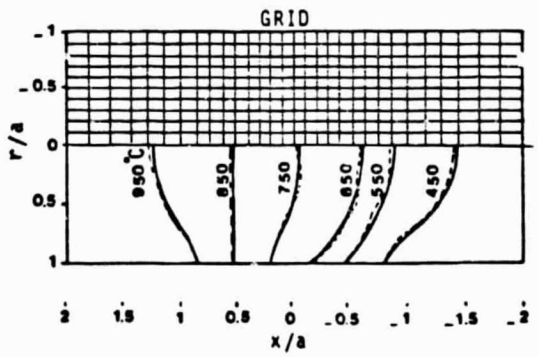

Two-Dimensional temperature distribution

Figure 4: Comparison between Analytical and Continuum's Solutions

_____ Analytical, Reference(5)

---------- Continuum

In the second group of runs (Runs #3, 4, 5), the effect of the furnace temperature distribution is investigated. Composition and boundary condition calculations, as described in the preceding sections, are invoked. The melting point temperature is 979 $^{\circ}K$ and the growth rate is 6×10^{-6} cm/sec. The rest of the parameters are as mentioned earlier. The hot and cold furnace temperatures, and the steady state temperature contours within the alloy are given in Figure 5 . It is clear that the furnace temperatures have a great effect on the location and curvature of the alloy's isotherms.

The third group of runs (Runs #6, 3, 7) shows how the alloy's steady state isotherms are affected by the rate at which heat is exchanged between the alloy and the furnace. This rate is controlled by the magnitude of the radiation coefficient, H_r, and the width of the air gap, δ_a . A smaller H_r means less radiative exchange while a smaller δ_a causes larger conductive exchange to occur. The values of H_r and δ_a for the three runs are given in Figure 6 and indicate that energy exchange is most efficient in Run #6 and least efficient in Run #7. Run #3 uses the real value of δ_a and the value of H_r estimated in the preceding section. Concerning the "efficiency" of heat exchange at the boundary, Run #3 is intermediate between Runs #6 and 7. For all of the three runs, the hot and cold furnace temperatures are 1099 $^{\circ}K$ and 788 $^{\circ}K$ respectively. The growth rate is 6×10^{-6} cm/sec and the rest of the input parameters are as mentioned earlier. The steady state temperature distributions are shown in Figure 6 and compared to the constant temperature distribution of the furnace. As expected, the wall temperatures of Run #6 are closer to the furnace temperatures than those of Runs #3 and 7. The temperatures at the cylinder's axis show the same behavior but to a lesser extent.

The last group of runs (Runs #4, 8, 9) shows the effect of the growth rate on the alloy's temperature balance. In all the three runs, the hot furnace temperature is 1273 $^{\circ}K$ and the cold temperature is 673 $^{\circ}K$. The radiation coefficient is 1079×10^{-8} gm/sec^3 $^{\circ}K^4$ and the width of the air gap is 11.5 mm. The growth rates of the three runs are given in Figure 7 along with the corresponding temperature contours at the steady state.

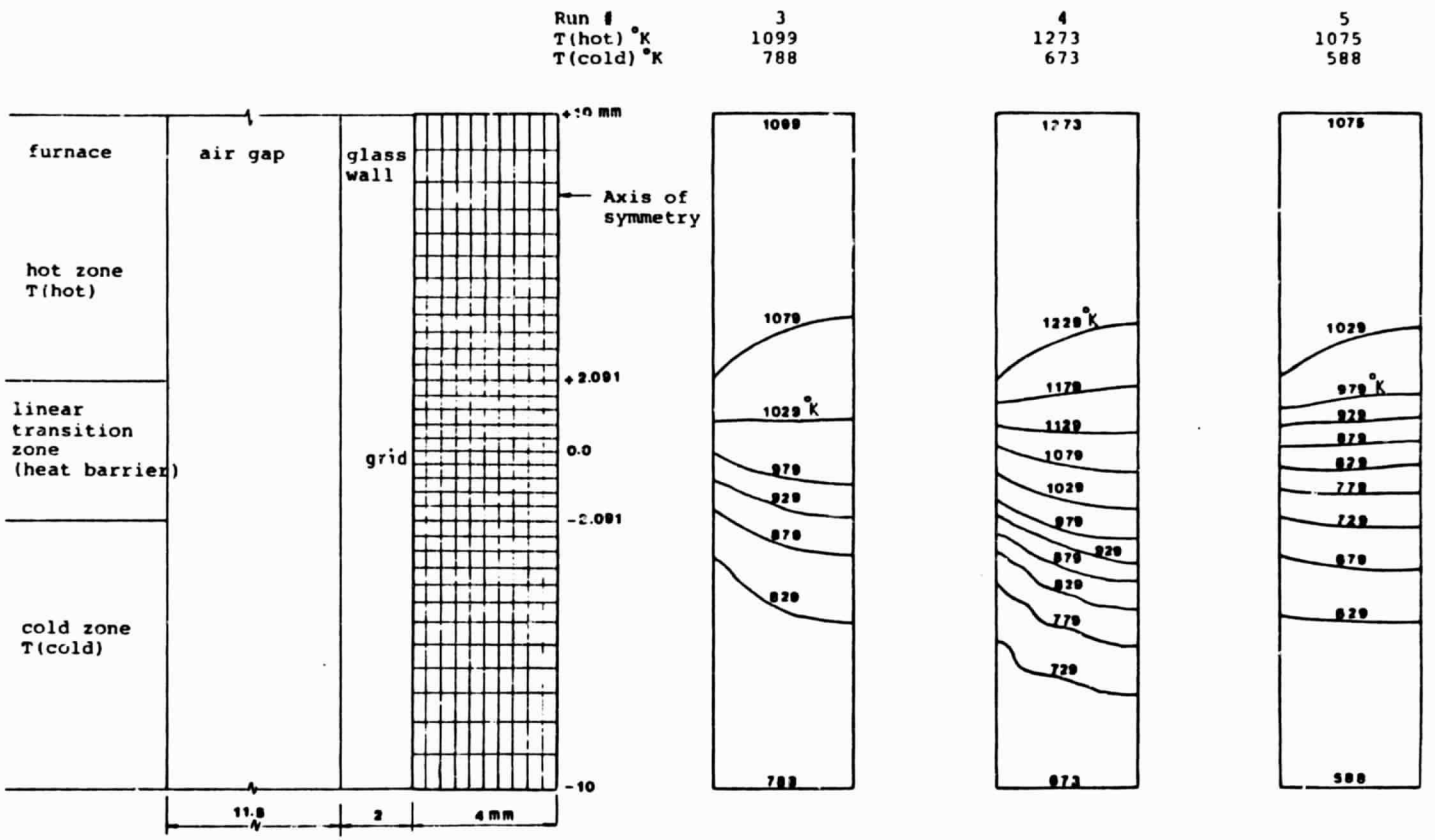

Figure 5: Effect of furnace temperatures on the alloy's steady-state temperatures.

Run #	6	3	7
H_r (gm/sec^3 °K^4)	1079 x 10^{-8}	1079 x 10^{-8}	1079 x 10^{-8}
δ_a (mm)	0.5	11.5	11.5

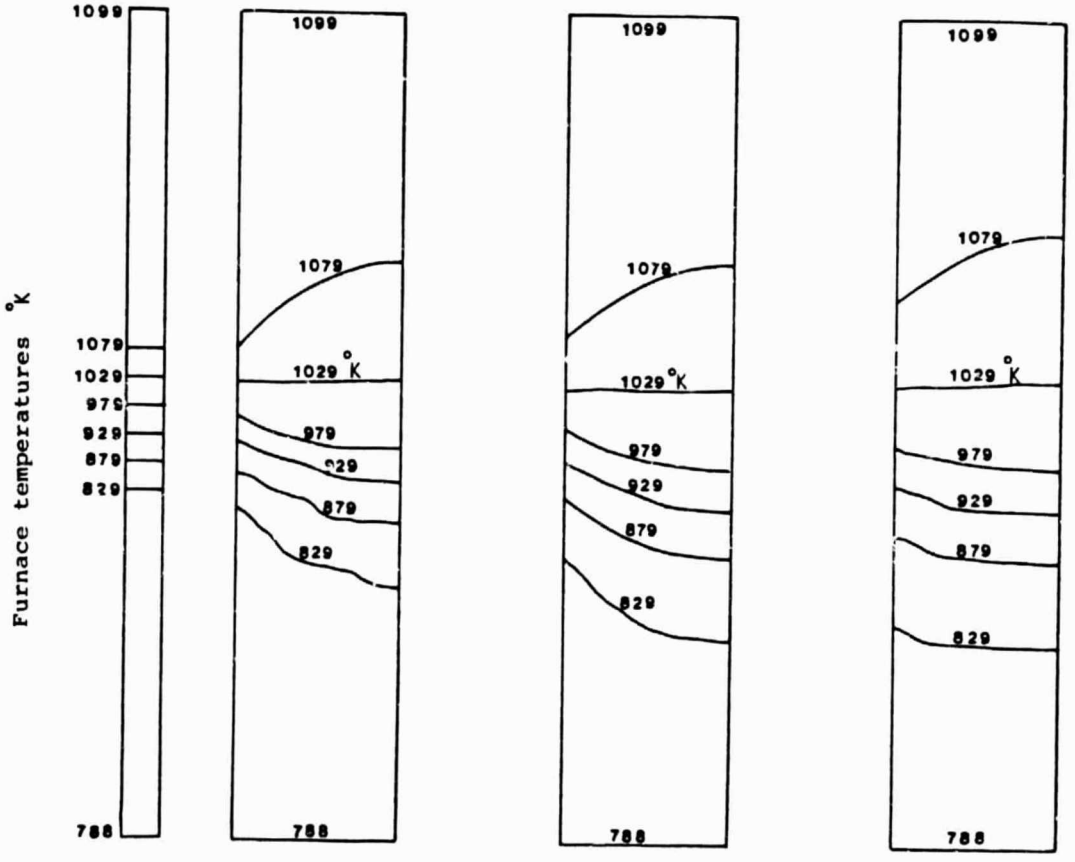

Figure 6: Effect of boundary conditions on the alloy's steady-state temperatures.

Run #	4	8	9
Growth rate (cm/sec)	6×10^{-6}	100×10^{-6}	3000×10^{-6}

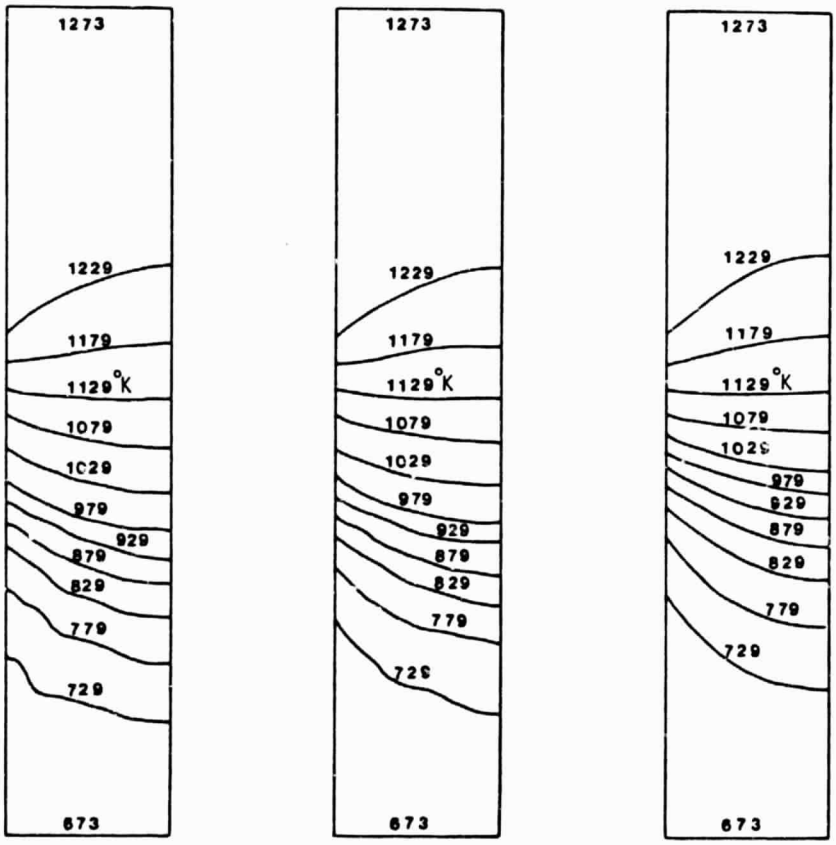

Figure 7: Effect of growth rate on the alloy's steady-state temperatures.

DISCUSSION OF RESULTS

The comparisons shown in Figure 4 demonstrate the accuracy of the numerical model used to simulate the Bridgman cell. The modest grid density used for these calculations causes no significant error in the results. Notice that no heat flux is predicted across the cell centerline, although no explicit specification of zero gradients is imposed on the centerline.

The cell model used assumes that solidification occurs on the 979 $^{\circ}$K isotherm. The hot and cold temperatures which are chosen for furnace operation move the melting isotherm, and, as shown in Figure 5, the shape of the isotherm is determined by where it is positioned in the cell. The heat transfer boundary conditions obviously control the isotherm location. Even though the individual boundary condition specification can be made more accurately, it is apparent that the interface shape can be controlled by furnace operating conditions. For the radiation boundary conditions and system physical properties used, Figure 6 shows that the interface is only slightly affected by the radiation and conduction levels. A more precise radiation analysis in the vicinity of the heat barrier region and a more accurate radiation/conduction analysis in the glass wall may affect the interface shape; such studies are in progress, but no results are available at this time.

The relationship between interface shape and growth rate is shown in Figure 7. This effect is small, even though isotherms away from the interface are markedly affected by the growth rate. Exact heat transfer boundary conditions in the barrier zone region will have some effect on the growth rate dependence of the interface, but the major effect is the neglected heat of fusion which is directly proportional to the growth rate. The experimental studies reported in (3) show flat interfaces for $H_g/C_d/T_e$ systems for very slow growth rates and curved interfaces for all of the larger growth rates conditions. The effect of composition alone does not appear to explain radial variations of interface shape because conductivity changes only slowly from the solid value at near interface locations in the liquid. Further analyses of both composition and thermal effects which occur on solidification are the subject of ongoing research.

CONCLUSIONS AND RECOMMENDATIONS

Thermal modeling studies of the Bridgman cell allow us to make the following conclusions.

1. An accurate thermal model of the Bridgman cell has been developed.

2. Less complete thermal models of the Bridgman cell, even if they include convective flows, cannot provide accurate simulations.

3. More detailed analyses of radiation effects in the vicinity of the thermal barrier and of the temperature distribution within the glass wall, along with better furnace wall and alloy surface radiation data, would improve the accuracy of the thermal model.

4. A better description of the concentration gradients and heat of fusion releases which accompany solidification would improve the thermal analysis.

5. The interface shape control methods reported in (2) can be quantitatively evaluated with Continuum's Bridgman cell model.

It is recommended that:

1. The radiation analysis at the barrier and the conduction analysis within the glass wall be extended to include details with regard to view angles and conductive node points in the glass.

2. The species conservation equation with attendant interface species and energy boundary conditions be included in the thermal model.

3. A wider range of parametric studies be made.

4. The thermal and solutal convection effects be included in the thermal analysis of the Bridgman cell.

REFERENCES

1. Farmer, R.C., "Mercury-Cadmium-Telluride Crystal Growth Investigation: Solidification Simulation", Final Report on NAS8-35049 by Continuum, Inc. (June 1983).

2. Szofran, F.R. and S.L. Lehoczky, "A Method for Interface Shape Control During Bridgman Type Crystal Growth of Hg Cd Te Alloys", Space Science Laboratory Preprint Series No. 84-132 (May 1984).

3. Lehoczky, S.L. and F.R. Szofran, "Directional Solidification and Characterization of Hg Cd Te Alloys", in Materials Processing in the Reduced Gravity Environment of Space, ed. G.E. Rindone, Elsevier Science Publishing Company, pp. 409-420 (1982).

4. Szofran, F.R. and S.L. Lehoczky, "The Pseudobinary Hg Te / Cd Te Phase Diagram", J. Electronic Materials, 10, p. 1131 (1981).

5. Naumann, R.J. and S.L. Lehoczky, "Effect of Variable Thermal Conductivity on Isotherms in Bridgman Growth", J. Crystal Growth, 61, pp. 707-710 (1983).

6. Cothran, E., personal communication (1984).

7. Welty, J.R., Wicks, C.E. and R.E. Wilson, Fundamentals of Momentum, Heat, and Mass Transfer, Second Edition, John Wiley & Sons, pp. 453-455 (1976).